SPE-209762-MS

# Tailoring Digital Approaches for Monitoring and Predictive Diagnosis for Sucker Rod Pumping Systems

Ngoc Lam Tran, Hamidreza Karami, Opeyemi Bello, and Catalin Teodoriu, University of Oklahoma



This paper was prepared for presentation at the SPE Artificial Lift Conference and Exhibition - Americas held in Galveston, TX, USA, 23-25 August 2022.



## Abstract

Sucker-rod pumps (SRP) are the most common form of artificial lift in depleted oil wells. Given vast datasets collected from years of operation, many operators are enacting digital technology to generate automated artificial lift systems. However, their online monitoring and optimization come with many challenges. Therefore, the individually engineered artificial lift is an imminent solution for long-term production, while maintaining cost efficiency. The key to make sucker-rod pumps operate effectively lies in downhole condition diagnostics. The emerging big-data analytics have provided relatively precise downhole condition forecasting based on available data, enabling better decision making. This study focuses on developing a testing digital SRP application, while leveraging analytical approaches to diagnose its operational anomalies.

This study presents an experimental and analytical workflow to monitor sucker-rod pumps and perform diagnostics using a designed Interactive Digital Sucker-Rod Pumping Unit (IDSRP). This unit consists of a vertical 50-ft long facility with a downhole rod pump at the bottom and proper instrumentation, capable of simulating a rod-pumped wellbore's operation. A linear actuator is used to provide the rod string's reciprocating movement and simulate different surface units and operating scenarios. The system utilizes the application of Pulse-width Modulation (PWM) technique and data-acquisition system (DAQ) to obtain analog results through signals detected by sensor. The surface dynamometer cards, and time-driven pressure and rate data are collected to train a cloud-based analytics software platform. The wave equation of Gibbs is used to draw the downhole pump card from the surface card. Some of the tested scenarios are normal pump operation with varying rates and varying levels of pumping off at the pump inlet.

The applied online prototype is designed to provide a step towards digitized automation systems. The setup is used to generate datasets for the rod-pump's operation at varying pump speeds, stroke lengths, and rod movement profiles. The collected data include the flowrate, bottomhole and surface pressures, and the dyno cards. The digitized transformation algorithms develop these physics-based inputs to generate predictive models, thus classifying operational conditions or failures of the pump. The model dynamically categorizes the pumps into key states of ideal condition and over-pumping with a regression fit accuracy of higher than 0.7 and overall classification accuracy of 92%.

The novelty of this setup consists not only of its mechatronic design but also allows thorough performance monitoring of the pump, thus easily validating models. The results have the potential of becoming a tool to optimize and shorten the downtime for repairing pump failures.

## Introduction

In order to recover more reservoir fluids to surface, artificial lift serves the purpose of providing sufficient pressure for the fluids to be able to push them to the wellhead. Sucker-rod pump or beam pump is one of the most common artificial lift methods for delivering oil production. With a lifting mechanism of exerting mechanical energy, the sucker-rod pump is considered an effective and simple alternative in the onshore fields operating at low pressures. This mechanical lifting method also suits for majority of fluids that have high reservoir temperature and are viscous. Moreover, the setup requires minimal cost when changing to other wells. However, the mechanical setup could result in several difficulties such as excessive friction in a deviated wellbore, solids handling, gas interference, and depth limitation due to rod capacity.

Given its operational pros and cons, monitoring conditions for sucker-rod pump is essential in sustaining producible operations. One of the common methods is to extract the surface dynocard, which records rod displacement and load or axial force in a full cycle. By looking at the dynocard, the operator can monitor the operation and identify the pump faults (Tripp 1989). For making accurate identification for rod pump condition in downhole, an algorithm was developed to convert the surface card to the downhole one by utilizing damped-wave equation calculations (Gibbs & Neely 1966). The axial force on the rod string represents the stress wave and thus the sucker-rod pump movement physically resembles of a 1-D wave propagation. The Gibbs wave-equation for downhole card calculation was later improved by utilizing a finite-difference model. The modified Everitt-Jennings model allows the calculation of space and time discretization, computing stress at any finite difference node (Everitt & Jennings 1992). The modified algorithm also considers the iterations of damping, fluid load line, and pump fillage calculation, resulting in more accurate downhole data (Pons 2014). The equations are derived to predict the pump behavior, including fluid dynamics and kinematic of rod pumping unit. The original works from Gibbs enable 20 different pump conditions detected through the downhole dynocard analysis. From then, down-hole dynocard became a generic workflow to identify possible sucker-rod pump working conditions and failures such as normal condition, fluid pound, shallow friction, leaking in valves, or gas interference.

With long-term usage resulting in large data collection, the acquisition and transmission process of surface and downhole dynocards must be transformed from manual to automated. The detection, diagnosis, and prediction of events leading to system down-time and sub-optimal performance are leveraged by the analysis of subject matter experts (Pennel, Hsiung, and Putcha 2018). However, this manual and time-consuming process is outdated. The pattern recognition method was developed by computer-based systems, which enables the surveillance for hundreds or thousands of wells (Albada et al. 2020). This method includes 2 processes of feature extraction and classification. The Fourier-series method was developed for feature extraction, where the algorithm helps filter noise in the pump displacement and recover the sinusoidal behavior in rod displacement and adds noise harmonic in pump load to recover rod load in the downhole (Chen 2018 et al.).

Numerous pattern-recognitions workflows involve classification techniques, supporting more proactive decisions. The common approach of classification technique is to implement mathematical tools for similarity observation. These tools are supported by numerical descriptors, and are summarized in Table 1.

**Table 1—Previous works employing mathematical functions to categorize the similarity in sucker-rod pumps**

| Authors (year) | Methodology | Classifier | No. of faults detected | Samples |
|---|---|---|---|---|
| Dickinson & Jennings (1990) | Grid method<br>Space features | Cost function | 7 | Dynamometer card limited in 7 wells |
| Lima et al. (2012) | Centroid<br>Curvature descriptor<br>K-curvature | Euclidean distance<br>Pearson correlation | 5 | 1500 cards |
| Yu et al. (2013) & Chen et al. (2018) | Fourier descriptors<br>Geometric vector<br>Level matrix | N/A | N/A | N/A |

Machine learning and artificial intelligence algorithms can be employed to train the computer-based models. The objective of these algorithms is to partition feature space into class labeling. Two approaches for solving classification problems are supervised learning and unsupervised learning. The first rule-based expert system to diagnose rod pump unit operation was developed by Derek et al. (1998). Afterwards, a variety of classifier techniques were explored, including artificial neural network (ANN), support vector machine (SVM), AdaBoost, and Bayesian network. A self-organizing map network, a technique to classify labels based on multi-dimensional components and proposed by Peng et al. (2007), classifies five pumping operational categories with the load values as the features. A semi-supervised model, combining Decision Trees, Bayesian Network, and SVM, was trained to predict rod pump failures (Liu et al. 2010). A Bayesian Network model, coupled with AdaBNet boosting algorithm, was trained with different weights to define the stronger boosted ensemble model to predict rod pump failures (Liu et al. 2011).

The prowess of artificial neural network (ANN) was furthered in subsequent works from Martinez et al. (1999), Osman et al. (2005) and Mohammadpoor et al. (2010) to predict the bottomhole pressure in oil wells or to analyze downhole dynamometer cards. Backpropagation neural network (BPNN) and SVM approaches were trained in 300 samples to diagnose 9 pump operating conditions (Rogers et al. 1990, Nazi et al. 1994). The input produces associated output that can identify the pump faults. A variety of ANN algorithms are described in the work of Bogulawski et al. (2018) providing the automated pattern recognition for rod pump abnormal state recognition. An improved ANN model, which is determined by a genetic algorithm, is furthered by the works from Abdalla et al. (2020) and Rashidi et al. (2010). Further heuristic search approach for pattern recognition and classification is also implemented in Liu and Patel (2013), which uses the maximum load during upstroke as a feature to differentiate the failures. The study identifies the well failure with 82-86% of positive prediction and only 11-15% of false alarm.

Table 2 summarizes some other previous works that apply machine learning. The drawback of deploying deep learning lies in the requirement of complex data engineering programs for image processing. The operators utilize different proprietary software that cannot be adapted in public or classroom settings. No existing literature in artificial lift mentions the possibility of generating models that learn from multiple operational parameters to predict the performance of pump. Therefore, the discussion of data-driven model prompts this study to explore a less complex real-time machine learning model that can learn from the multivariate operational inputs to establish the predictive mode. This is helpful for anomalies detection when the test points fall out from the established trends.

Table 2—Some of the previous studies applying machine learning algorithms for rod pumps

| Authors (year) | Features | Classification Algorithm | No. of faults detected | Samples | Results |
|---|---|---|---|---|---|
| Liu et al. (2011) | Card area production, daily run time, stroke per minutes, etc | Semi-supervised learning with AdaBNet | 4 | 100 cards | Accuracy 90% |
| Xu et al. (2007) | Space feature points | Unsupervised learning, self-organizing map | 5 | 6377 cards | Accuracy 93.4% |
| Liu et al. (2010) | Multivariate timeseries Card area, daily tun time, cycle, approved oil production rate | Decision Tree SVM Bayesian Network | 6 | 42 train wells 32 test wells | Error rates 0.008 to 0.029 |
| Bezerra et al. (2009) | Space features | Supervised learning BPNN | 8 | 300 | Classification error=1.31% |
| Abdalla et al. (2020) | Dynamometer cards | ANN with genetic algorithm | 4 | 4467 | Precision and recall values 93.2% over all pump faults |

## Methodology

This study is an attempt to integrate an experimental Interactive Digital Sucker-rod Pump (IDSRP) facility and an analytical workflow to build an automated diagnostic systems for the rod-pump operational framework. A data-driven application is generated to become a prototype for artificial lift automation in the industry. Figure 1 highlights the overall experimental and analytical approaches implemented. The experimental setup is completed with the objective to mimic the operation of a sucker-rod pump in the field scale. A physical baseline model is implemented to correlate the actuator's speed with the linear reciprocating movement of the rod string, generating values similar to a field scale.

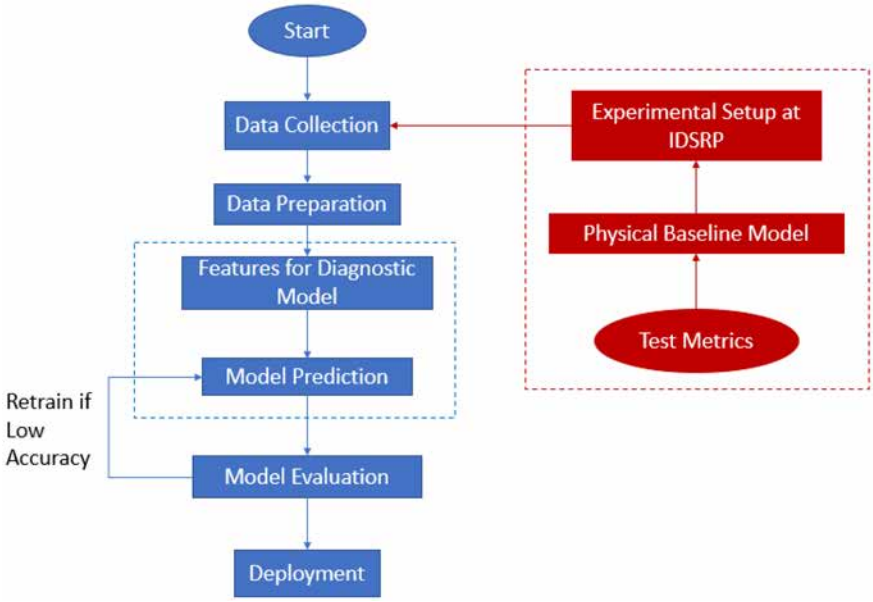


Figure 1—Workflow schematic utilized, combining experimental and data analytics approaches

The data obtained from the experiments are treated for feature selection in the diagnostic model. The treatment stage includes resolving missingness and handling outliers in the raw dataset. The feature engineering for the model is conducted by normalizing dependent and predictor variables (Eq. 1, Eq. 2). The dataset is split in a training set for model prediction and a test set for model evaluation. A hyper-

parameter selection stage is carried out to optimize the learning process. The model is retrained if the resulting evaluation parameters (i.e. accuracy) are lower than the common goals. The final stage involves the deployment of the workflow to detect the imminent performance of the rod unit.

$$Normalized\ x = \frac{x - x_{min}}{x_{max} - x_{min}} \tag{1}$$

$$Normalized\ y = \frac{y - y_{min}}{y_{max} - y_{min}} \tag{2}$$

## Experimental Design

With the rising application of the Internet of Things (IoT) in the upstream petroleum industry, the experimental design in this work attempts to integrate the physical model and cloud-based architecture. The design follows industrial standards and enables data manipulation through programmable units. The application of SCADA and programmable logic controller units is mentioned in the works of Pennel et al. (2018), Palmer and Turland (2016), and Boguslawski et al. (2018) to generate IoT databases. These databases generate the analytical solutions for automated dyna-graph card recognition while leveraging AI ensemble models. Following this idea, the IDSRP facility is designed to investigate the common field application using a variety of wellsite instrumentation such as force, stroke transducer, controller, etc.

The IDSRP is a 50-ft vertical facility that houses a linear actuator, load cell and polished rod in the upper frame, transparent casing, tubing, return line and rod string in the middle section, and downhole rod pump and liquid tank in the bottom section (Figure 2). The setup is designed to mimic and simulate a real wellbore's operation. The principal elements in this setup include the linear actuator and motor. The linear actuator provides reciprocating movement and simulates dyno cards with various operating scenarios. The resulting acceleration from transmitting the linear forces to the rod string impacts the dyno card's shape. The records from this setup are aggregated into an interactive digital solution, designed using the LabView environment. The user interface records all the sensors' readings and visualizes the pressure variations and dyno cards in real-time.

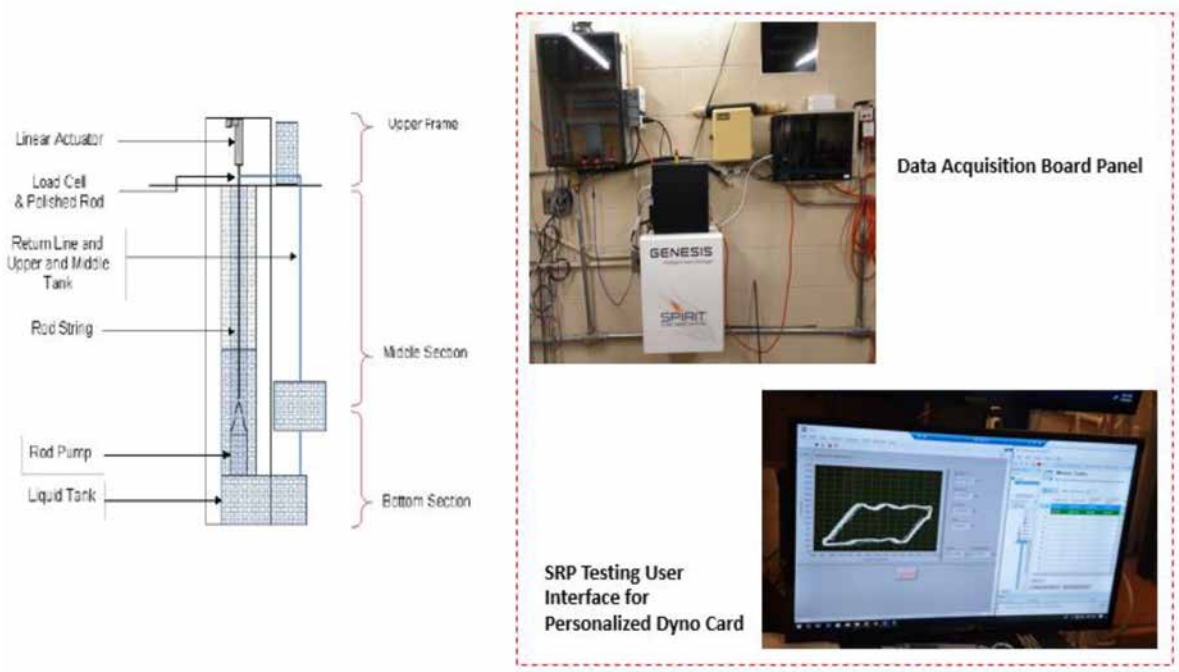


**Figure 2—Schematic of IDSRP facility, DAQ system, and user interface (Teodoriu et al. 2020)**

Three modes are involved in the IDSRP experimental setup. Together, these modes further the implementation of IoT principle in resembling field-scale operations and generating the AI model (Teodoriu et al. 2020).

1. The ***physical SRP mode*** focuses on the design and construction of a unique experimental SRP setup in the laboratory.
2. The ***offline mode*** to carry out experimental verification and performance testing. Each operation of the unit is carried out with the integration of physical SRP setup and digital SRP simulator in LabVIEW environment, enabling data transmission and acquisition from sensors. The integral components of the mode include linear actuator and fluid systems.
3. A real-time monitoring and diagnosis system is built in the ***online mode***. The graphical interface provides early warning and simultaneous monitoring for wells. The recorded surface dynamometer cards and time-driven data are processed and trained in a cloud-based analytics platform. The algorithm plays a role as a diagnostic model to determine the operating condition of the rod unit. The cloud-based analytical solution allows production optimization and improves the decision-making process for abnormality detection and immediate maintenance activities.

## Data Acquisition

The DAQ system is designed to collect data while operating the facility and recording measurements from sensors. The specifications for sensors applied in the IDSRP are described in detail by Sharma et al. (2021) and in Table 3. The accuracy of these sensors ranges from 0.25 to 0.5%. Noise reduction is considered through adding the low-pass, high-pass, or bandpass filters in the input line and testing these filters for inference, acquisition frequency, and sampling rate. This process maintains the clear signal input lines. The load cell sensor receives a live signal through a digital output, with the measurement decoded using the analog input port. Combining with motor sensors, these sensors form the load force and displacement components for a surface dynamometer card. The liquid level sensors detect the changes of liquid level in the top and bottom tanks. The encoder of the sensor also measures the rotation speed of the linear actuator. Once the motor is operated, the associated drive calculates the speed, acceleration, and position. The signal data recorded by these sensors are accessed and measured through the LabVIEW software.

**Table 3—Sensor specifications utilized in the IDSRP Facility (Sharma et al. 2021)**

| Device Name | WIKA C-10 | PSD S1 | TE Connectivity SP2-25 |
|---|---|---|---|
| Range | 0-100 psi | 0-220 lbs. | 0-25 inches |
| Excitation | 12 Vdc | 10-15 Vdc | 30 Vdc |
| Output range | 0-5 V | 2 mV | 94% ±4% of input voltage |
| Placement | Pressure Transducer, at upper and bottom sections | Load cell, at top of rod string | Displacement sensor, at rod string |
| Accuracy | % of span ≤ 1.0 (limit point calibration) | ± 0.5% | ±0.25% FS |

LabVIEW is a system engineering application software for testing, measuring, and monitoring data, utilizing a graphical programming approach to visualize all application features. The graphical block diagram visualizes the feedback of the system. The LabVIEW installation helps control the motor and linear actuator movements and supports the DAQ device in sensor data gathering. LabVIEW provides an interface for data gathering with the constant analog signal.

The Case Structure for data storage generates a 1-D array of data grouped by a displacement value and captures all data points in every iteration as fast as possible. The output file for LabVIEW is under

a coma separated-value structure, which can be parsed and programmed with the set of cloud software programming used in the study, including MATLAB, Excel, R, and Python. Continuing the proposed sensor data installation in the previous work of Pienknagura Dolberg (2019), the resulting visualization of force load and displacement data points in each iteration is displayed in Figure 3. The user can observe and monitor the positions, velocity, and changes of force and displacement with respect to upstroke and downstroke movement in the physical unit of SRP. The top and bottom tank levels are also shown in the interface to monitor the fluid flow in the closed loop and allow immediate action in case of leaks.

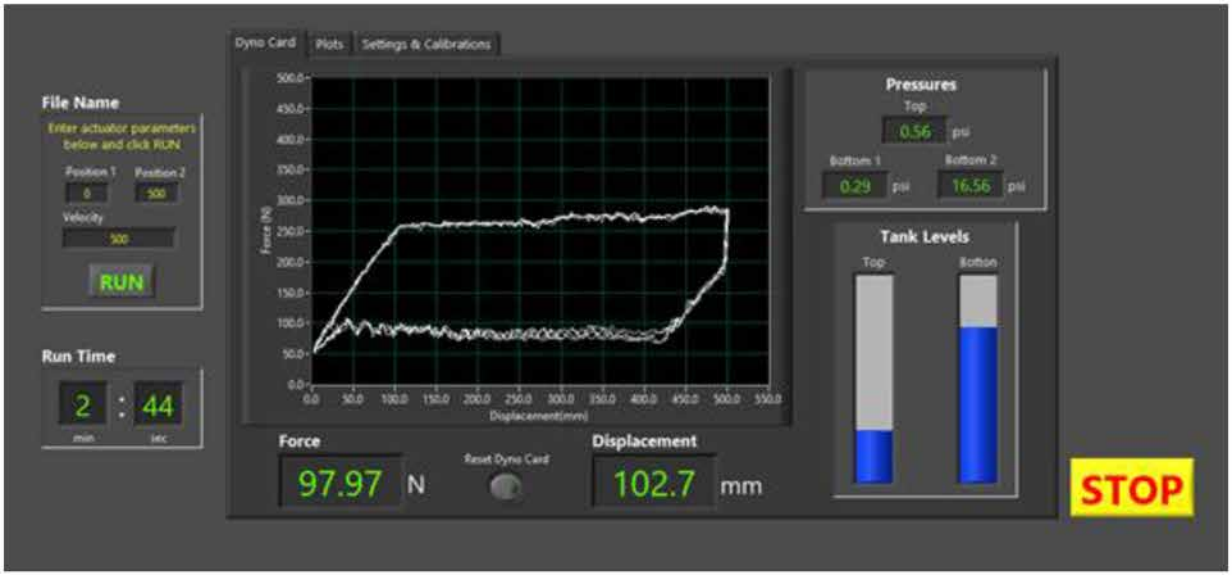


**Figure 3—The visualization of SRP unit in LabVIEW during the operation**

The testing procedure and data input in the LabVIEW interface follow the recommendations of Pienknagura Dolberg (2019). The cyclic stack of load and displacement curves shown during the procedure resembles the field SRP cards, which is helpful for the analytical solution in the online mode.

The designed test matrix for the testing procedure is described in Table 4. The operation of SRP is simulated in short-term and long-term tests (5-20 minutes), with different levels of actuator speed (RPM) and magnitude of rod movement (stroke length). A linear baseline model is used to correlate the actuator's RPM and the rod pump's number of strokes per minute (SPM). The acceleration of the actuator is maintained at 167 rpm/sec. A successful test generates the surface dynamometer card of load force vs. displacement and pressure readings in the top and bottom of the rod-pump unit.

**Table 4—Current study's experimental test matrix**

| Stoke Length (mm) | Duration (min) | Actuator RPM | Shape | Acceleration (rpm/sec) |
|---|---|---|---|---|
| 150, 200, 250 | 5 to 20 | 500, 1000, 1500, 2000 | Trapezoidal and sinusoidal | 167 |

## Actuator Baseline Model

The experiments are carried out based on the relation between the pump's number of strokes in a minute and the linear actuator's RPM. The movement of the actuator is simulated with trapezoidal and sinusoidal designs. A trapezoidal shape reflects the ideal experimental condition with no noise and more rapid change of rod displacement, while the sinusoidal shape mimics the actual operational scenario with both harmonic displacement and noise involved. Figure 4 illustrates the linear correlation between the number of strokes per minute and the actuator's RPM for different stroke lengths. The difference between the figures lies in the input movement shape. The tests are carried out with the trapezoidal and sinusoidal shapes. Due to the

movement shape and lower peak accelerations, the sinusoidal design results in lower SPM values compared to the trapezoidal shape. Also, a higher stroke length generates a lower number of strokes or cycle over time for a fixed actuator RPM. The linear trends show a simplified correlation between these two factors that can be used to estimate the pump's speed based on the actuator RPM.

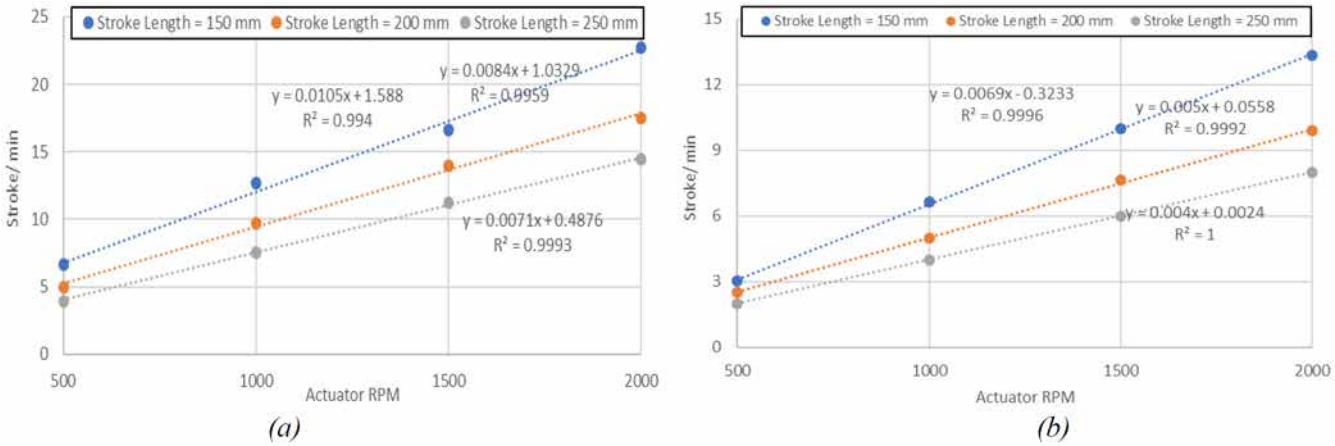


**Figure 4—Linear correlation between the pump SPM and actuator RPM for varying stroke lengths and (a) trapezoidal shape, (b) sinusoidal shape**

## Results and Analysis

### Pattern Recognition

The initial step is to resolve the outliers observed in the raw dynamometer card by using a z-score that indicates the vicinity of the data to the mean. The feature extraction and normalization are implemented as the data processing steps. The Gibbs wave equation is deployed to transform the surface card to a downhole one. The result is used for pattern recognition of the dyno card. From this, the operational condition of the SRP is determined. The implementation of Gibbs wave equation is based on the approach of Everitt-Jennings's work (1992). It is important to adjust the inputs for the wave equation such as the material properties (Young Modulus, density, length of rod string), and number of nodes, based on the laboratory conditions. The results will be used for pattern recognition.

The dynocard conversion algorithm is applied for a few sample cards extracted from the literature. The purpose of this comparison is to verify the conducted calculations and the developed algorithm. The sample cards are extracted from real field scales in the literature, as shown for a case in Figure 5. The left plot shows the surface and downhole cards picked up from the literature. The right plots show the comparison of the published digitized downhole card and the calculated one using this study's program. The percentage errors in the area under the curve between the real downhole cards and the calculated ones are analyzed to validate the model for two sample cases (Table 5). The errors are small and less than 1.5%, which justifies the confidence in the data and conversion algorithm.

**Table 5—Percentage errors between actual and calculated downhole cards for two samples**

| Sample | Error (%) |
|---|---|
| 1 | 0.74 % |
| 2 | 1.34 % |

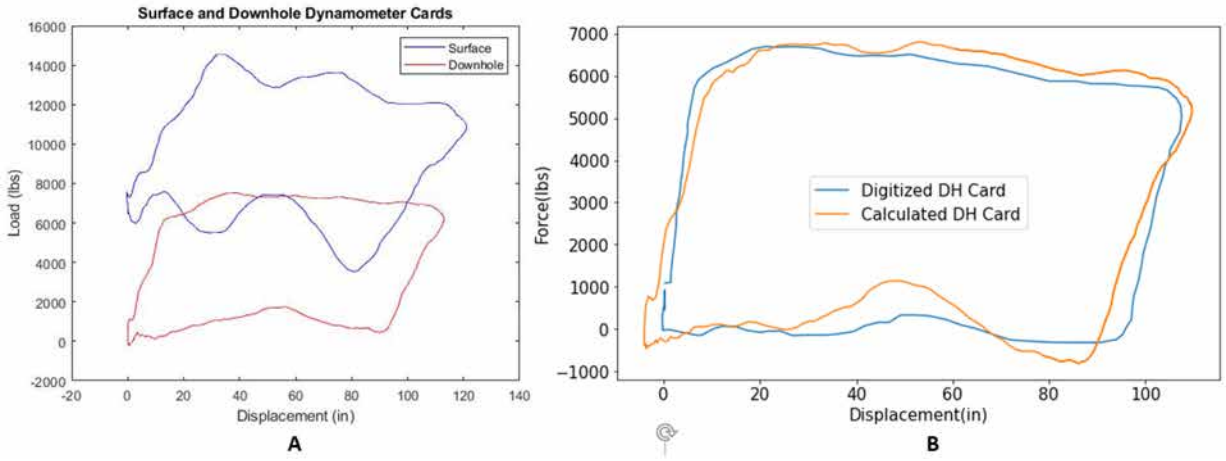


**Figure 5—(A) Extracted surface and downhole cards, sample 1 (Everitt, Jennings 1992, Ercolino 2011) (B) Actual (digitized) and calculated downhole cards comparison**

The surface to downhole dynocard conversion algorithm was applied to some sample cards obtained from the experiments in normal operating conditions. The results of the surface and downhole dynamometer cards are shown in Figure 6 and Figure 7. These cards are obtained with 250 mm stroke length and with 2 SPM and 4 SPM, respectively. The surface cards are selected from one cycle of the pump's operation. The converted downhole cards from these figures are shown in red.

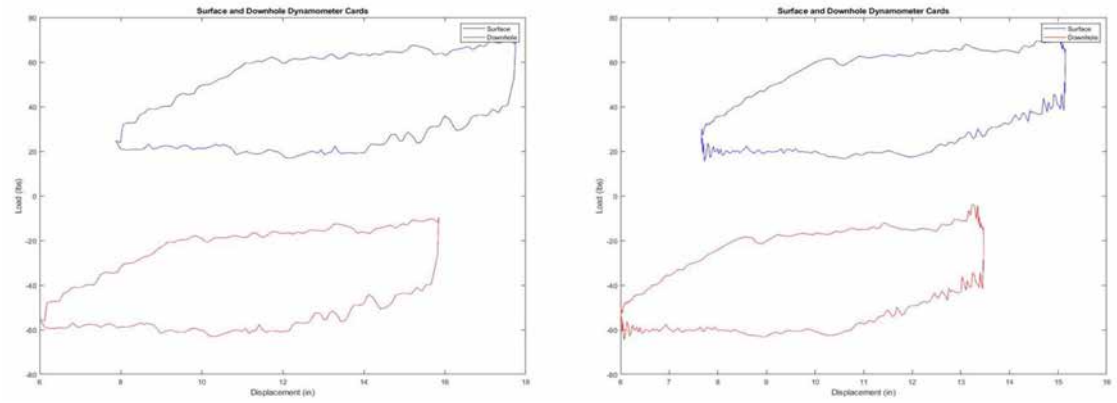

**Figure 6—Conversion of surface to downhole dynamometer cards with input stroke length of 250 mm and pump SPM of 4**

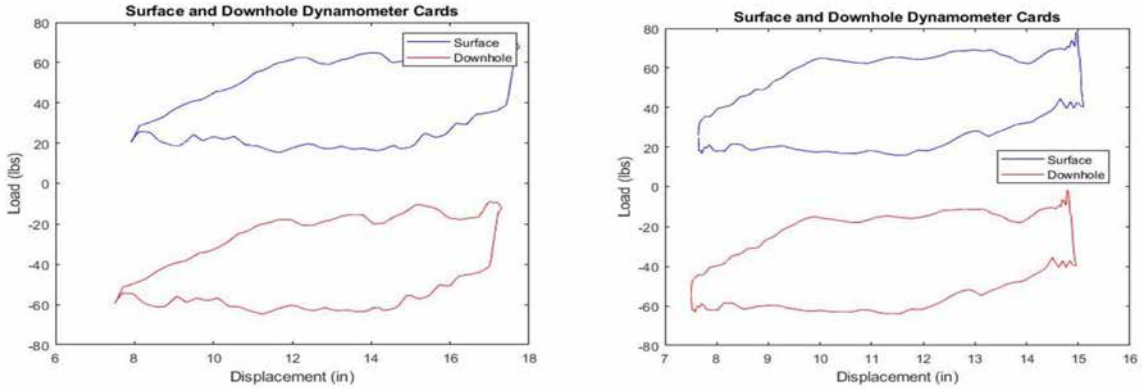


**Figure 7—Conversion of surface to downhole dynamometer cards with input stroke length of 250 mm, machine SPM of 8**

The noise and discrepancy during the transition from upstroke to downstroke are due to the lower modulus of elasticity and buckling in the rubber-like rod string of the experimental setup. The low modulus of elasticity affects the static elongation, where the natural vibration opposes the motion of the polished rod at the peak of the dynamometer card. Kendrick and Corneluis (1937) also described this phenomenon by observing the polished rod returning to the top of the stroke before completing the downstroke. The fluid pressure surrounding the rod string increases the magnitude of the compressive force that the rod string must support. A slim rod string can withstand a certain amount of compressive load before the buckling threshold, which results in contact between rod string and tubing (Lukasiewicz and Knight 2006). The abnormal rod string stretching or buckling may alter the shape of the dynocard compared to the field scale cases. As a result, the transformation may not be readily translated from the lab to field conditions.

**Preliminary Analysis**

The results from pattern recognition imply the need for a more time-driven analysis based on the parametric signal data processing. The pressure and movement data over time provide further insights about the pump performance, including force range, liquid flow rate delivered by the pump per cycle, differential and frictional pressure losses. These calculations help generate additional features for the model input. The changes of any of these features with time can be used to evaluate the SRP performance.

The plunger's mechanical properties and fluid properties are taken from the early model developed by Pienknagura Dolberg (2019) (Eq. 3 and Eq. 4). The formation volume factor ($B_o$) is 1, and the volumetric efficiency of the plunger is assumed to be 80% with water used as the testing fluid.

$$q = 0.1484\frac{A_p N S_p E_v}{B_o}\,(STB/D) \tag{3}$$

where $A_p$ is 3.167 in$^2$, N is the number of strokes per minute (SPM).

$$S_p = S - (e_r + e_t) + e_o \tag{4}$$

where $e_r$ = 0.0035, $e_t = 1 \times 10^{-6}$, $e_o$ =0.000015 (Pienknagura Dolberg 2019).

The pressure difference between the top and pump discharge sensors shows the flow's pressure drop along the vertical tubing (Eq. 5), where $P_T$ is the pressure record at the top sensor (psig) and $P_{B_2}$ is the pressure recorded at pump's discharge sensor (psig). The frictional pressure loss can be calculated by subtracting the hydrostatic column from the pressure drop (Eq.6). The resulting frictional losses are shown in Figure 8 with respect to flow rate, accounting for systematic and random uncertainties. As expected, frictional losses increase as the flowrate increases.

$$\Delta P = P_T - P_{B_2}(psi) \tag{5}$$

$$\Delta P_{\text{friction}} = \Delta P - P_{hydrostatic} \tag{6}$$

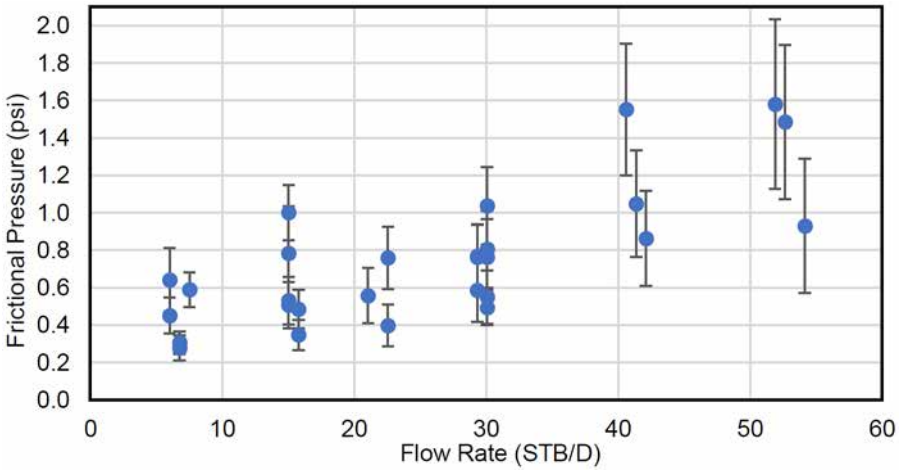


**Figure 8—Frictional pressure losses with respect to liquid flow rate delivered by the pump**

The suction pressure recorded at the first bottom sensor provides the information about the level of water column pumped at the intake. The changes in the hydrostatic column of water can be inferred from the difference between maximum and minimum section pressure values recorded during upstroke and downstroke (Eq. 7 and Eq. 8). The frictional pressure results are significantly smaller than the hydrostatic pressure column, as seen in Figure 8, and can be neglected for this estimation. Figure 9 reveals the changes in intake pressure ($\Delta P_{B1}$) and resulting water column per cycle at the pump intake with respect to liquid flow rate. The data are scattered in the plot because flow rate is a function of both stroke length and SPM, while water column primarily depends on stroke length. The generalized linear regression (GLM) is added to improve the fitting. The larger changes of intake pressure mean a higher column of water fed into the system during the upstroke, thus a higher flow rate.

$$\Delta P_{B1} = P_{B_1 max} - P_{B_1 min}(psi) \tag{7}$$

$$Water\ Column\ at\ Pump\ Intake\ per\ Cycle = \frac{\Delta P_{B1}}{0.433}\ (ft) \tag{8}$$

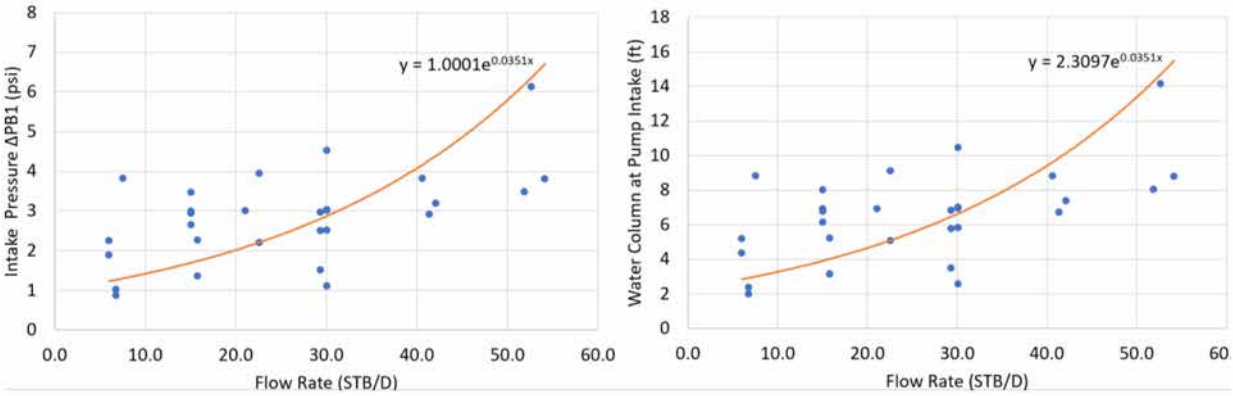


**Figure 9—Suction pressure range and resulting water column pumped per cycle at the intake**

The range of rod load is calculated as the difference between the peak load achieved on the upstroke and the minimum load recorded on the downstroke (Eq.9). This feature is an important parameter for the predictive modeling identifying the ideal conditions.

$$\Delta F = F_{max} - F_{min}(N) \tag{9}$$

## Physics-based Labeling

When the SRP operates in a continuous normal mode, it maintains steady-state conditions with constant pressure, continuous inflow into wellbore and fluid lifted to the surface (Rowlan and McCoy 2018). Due to the instability of SRP operation, deviation from normal mode alters the consistent trend of parametric features with time. As the rod speed (SPM) can be the driving factor to determine pump operations, impacts of rod motion speed are analyzed to divide the tests into normal and pumping off cases. Based on Figure 10, an increase in rod speed (SPM) alters the suction pressure trends and the resulting water column filled at the pump intake. As time goes by, the high rod speed removes an excessive amount of liquid in the casing annulus, while the liquid recirculation to get back into the suction point is not as fast. This hence reduces the B1 (suction) pressure ranges and the intake liquid column level with time. As a result, the suction pressure and liquid column fall off from the constant trend with time. This results in a potential incomplete pump fluid fillage. Before training the predictive mode, the pump cards for various tests were categorized using the intake pressure trends with time throughout the test. The tests with a negative slope of intake pressure with time were labelled as pumping off cases.

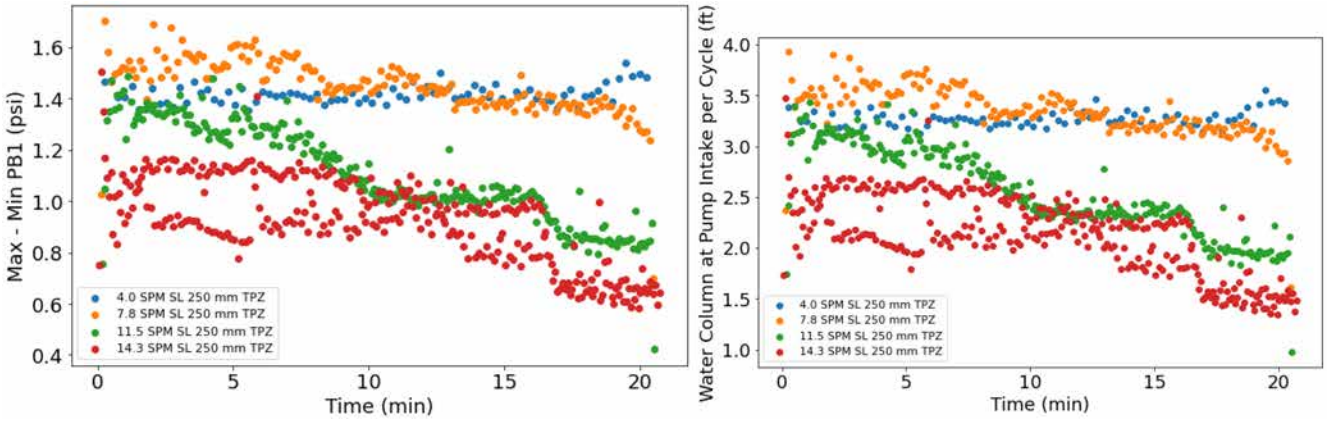


**Figure 10—The difference of maximum and minimum intake pressure (B1) and resulting water column at pump intake per cycle, with 250 mm stroke length and trapezoidal shape**

Figure 11 provides the SPM values corresponding to the linear actuator's RPM for the tests conducted with varying stroke lengths. Tests are divided into five levels of SPM values, including highest, upper high, middle, lower, and lowest SPMs. There is no single factor determining pump-off in SRP operations. Grouping the tests based on only SPM values does not fully encompass other factors, such as displacement shape or stroke length. Therefore, the product of speed (SPM) and stroke length is used as the proportional length of liquid column filled per minute. Using this parameter establishes a threshold to determine the possibility of pumping off. If the total length of the water column getting pumped at a given time exceeds the feed water supply, the water level at the pump intake decreases. This occurrence reduces the suction pressure over time, and pumping-off may occur.

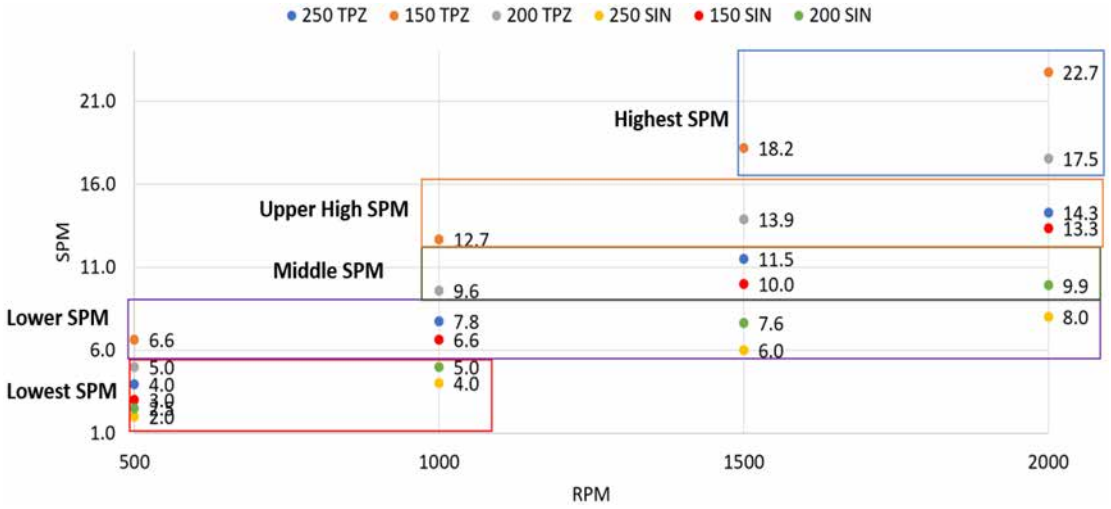


**Figure 11—Five levels of SPM values based on SPM vs. RPM plot**

A linear regression fitting was used to find intake water column level vs time slopes in the five SPM groups. A more negative slope is observed if the pump card indicates early pumping-off signs. As the water column depends on the intake pressure through Eq. 8, only the results of the intake water column plots are shown for the five SPM groups in Figure 12. There are slight instabilities observed in a few pump cards at upper high and lower SPM groups. Despite slight declines in production with time, the amount of water filled at pump intake is maintained relatively constant for SRP systems operating at lower speed groups.

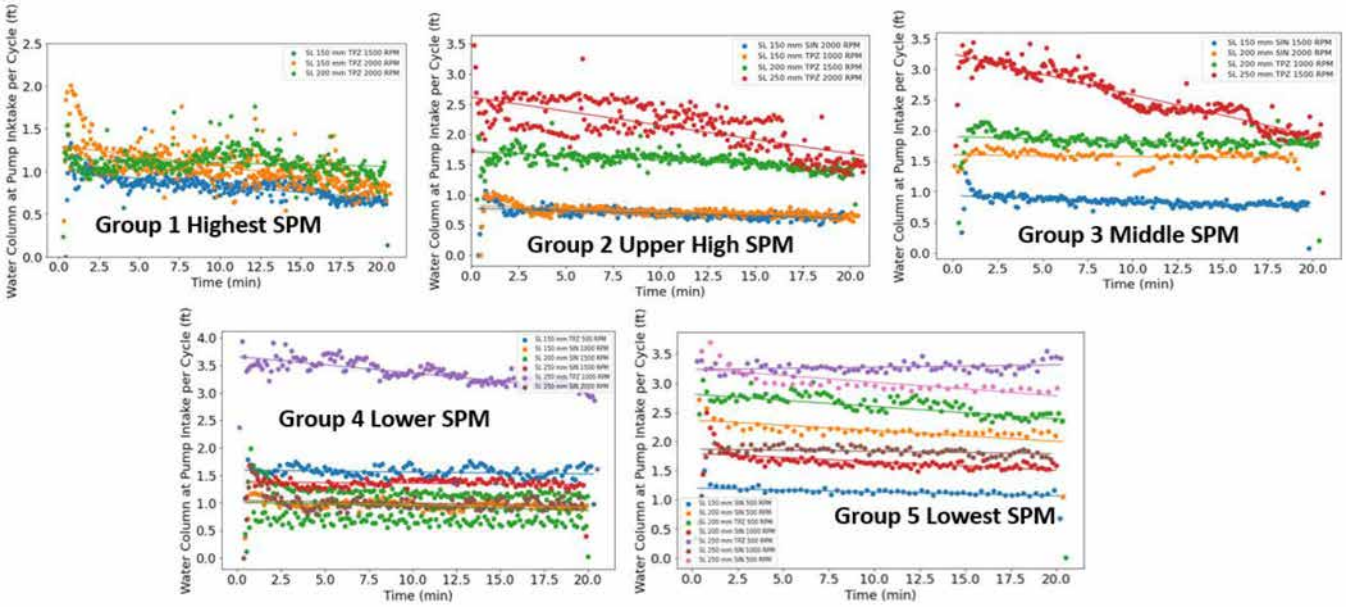


**Figure 12—Samples of regression fit for water column at pump intake per cycle with time for the five tested SPM groups**

The water column length being pumped per time can be estimated as the product of the stroke length and the pump's SPM. If this factor exceeds 2000 mm/min, more anomalous cases are observed with more negative slopes. Threshold of -0.024 was selected for the slope of the intake water column vs time to differentiate the normal operation and pumping off. With this threshold, four of the tested cases fall in the pumping-off region. The objective for building a machine learning model is to create the predictive regression-based and classification models to predict normal operation performance and detect the abnormal cases.

## Label Validation

As the regression model differentiates between normal and anomalous cases, the set of inputs from slightly pumped-off cases trains the model to determine whether the test deviates from the expected normal operation. The data from slightly pumped off cases are used as diagnosis cases to detect the abnormality.

Following the algorithm discussion, the models are trained with the experimental inputs, including shape, RPM, SPM, stroke length, and test duration. Table 6 summarizes the evaluation metrics on validation data for the three MIMO regression techniques. These metrics denote the capability of the models to fit and predict accurately. Due to the ability to utilize distance-based calculation to navigate the neighborhood, KNN performs the best. It shows a better evaluation score in predicting output values compared to the other two techniques, with the 0.87 goodness of fit and relatively low errors.

**Table 6—R-2 evaluation score and explained variance of validation data for 3 multiple-input multiple-output regression techniques**

| Technique | R-2 Evaluation Score | Explained Variance |
|---|---|---|
| Linear Regression | 0.54 | 0.54 |
| K-nearest Neighbor | 0.87 | 0.87 |
| Decision Tree | 0.78 | 0.78 |

The predictions of the three models are compared to the SRP features over time for a test with normal conditions, as shown in Figure 13. The predicted results from KNN and DT are relatively close to the actual normal operation data. The visual observations imply that Linear Regression does not perform well due to the linear relationship assumption, which fails to adopt the cyclic nature of the raw data.

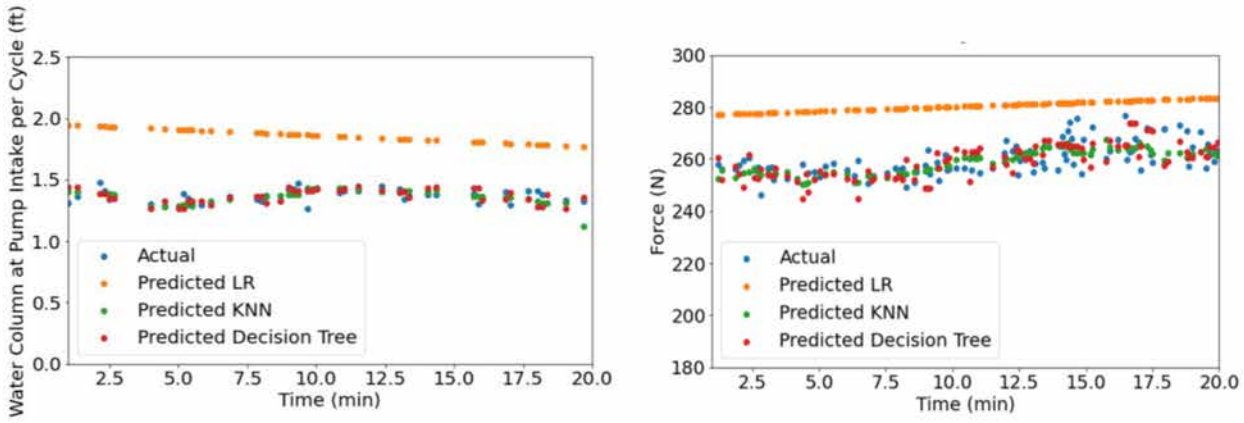


**Figure 13—Visual comparison between the true (actual) normal operation data and the predicted trends of machine learning models**

The trained model is deployed in the slightly pumped-off data. In this case, the prediction differentiates actual normal and slightly pumped-off operations based on the same sets of experimental inputs. In the testing stage, KNN and DT models are selected based on the evaluation results, as shown in Table 7. Figure 14 exhibits the distinctive trend between normal and abnormal operations. The evaluation metrics include the negative R-squared of -3.56 for KNN and -4.78 for Decision Tree, and significant errors. The quantitative measurement implies that the pump-off cases do not follow the predicted trends of normal operations. The predicted constant intake pressure and constant intake water level confirm the underlying physical basis in these MIMO regression models. In this case, the abnormal operation is detected when parametric performances of slightly pump-off cards deviate from the diagnostic plots of forecasted models. Overall, these predictive models can be applied to any experimental input set to diagnose the pump operation and monitor the early signs of abnormal occurrences (i.e., pumping-off issues) in IDSRP.

**Table 7—Mean Absolute Error (MAE) and Mean Squared Error (MSE) metrics of validation data of multiple outputs for regression techniques**

| WC at pump intake (ft) | MAE normal operation | MAE abnormal operation | RMSE normal operation | RMSE abnormal operation |
|---|---|---|---|---|
| KNN | 0.10 | 0.892 | 0.18 | 1.046 |
| DT | 0.13 | 1.093 | 0.24 | 1.344 |

| Intake pressure range (psi) | MAE normal operation | MAE abnormal operation | MSE normal operation | RMSE abnormal operation |
|---|---|---|---|---|
| KNN | 0.044 | 0386 | 0.077 | 0.453 |
| DT | 0.06 | 0.473 | 0.1 | 0.581 |

| Rod load range (N) | MAE normal operation | MAE abnormal operation | MSE normal operation | RMSE abnormal operation |
|---|---|---|---|---|
| KNN | 14.12 | 53.89 | 9.32 | 63.249 |
| DT | 18.17 | 53.09 | 38.27 | 67.17 |

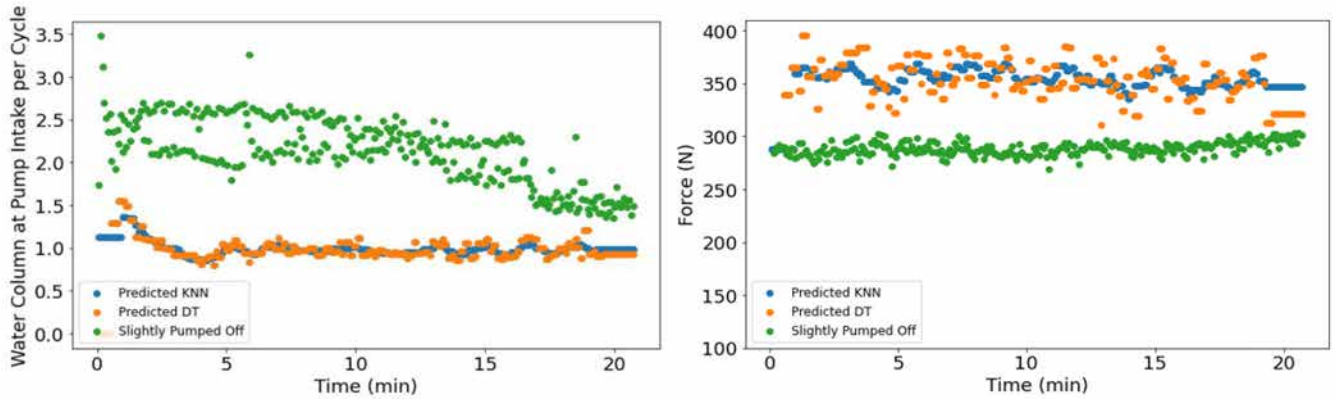


**Figure 14—Visual comparison between the slightly pump-off case and the normal operation predicted from KNN and Decision Tree**

## Parametric Threshold Testing

The regression approaches generate models to predict the normal performance of a SRP and detect anomalies. There is more confidence in quantifying the threshold parameters to identify the operational type of a pump card. The threshold parameters may be the stroke length and number of strokes per minute or the minimum slope of the intake pressure and the resulting intake water column over time. The last step is to carry out a comprehensive supervised learning model to classify the SRP's operation based on the experimental parameters. Apart from the given test matrix, four additional tests with random inputs are included in the dataset to ensure the volume and variety qualities for big-data applications. Therefore, the supervised classification approach incorporates data from 52 pump cards.

The labels used for the analysis are shown in Figure 15 with 40 normal cards or 4568 associated data points in Label 0, and 12 anomalous cards or 1741 associated data points in Label 1. The imbalanced data concern due to uneven distribution is addressed by up-sampling the minority class (i.e., Label 1) in the training set. The up-sampling technique prevents the model from bias prediction inclining towards the majority class (i.e., Label 0).

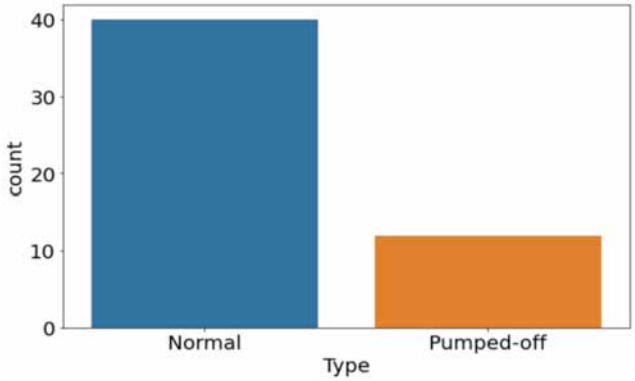


**Figure 15—Resulting labels for 52 pump cards obtained from IDSRP testing based on the slope of intake pressure with time**

As the output is binary, the four machine learning models include Logistic Regression, Decision Tree, Random Forest, and Gradient Boosting. Once these models are trained, the prediction is evaluated using the test data. Table 8 summarizes the evaluation for the four classification techniques. The accuracy metric represents the fraction of test data predicted correctly. Precision indicates the confidence level in the cases predicted as Label 1 (i.e., abnormal case). Recall indicates the ratio of true abnormal cases (Label 1) identified by the model. F-1 score is a harmonic mean of precision and recall. The marginal overall accuracy metric implies the robustness of these classification techniques in determining normal and slightly pump-off cards.

**Table 8—Different evaluation metrics on test dataset for supervised classification methods**

| Methods | Overall Accuracy | Precision | F-1 score Label 1 | F-1 score Label 0 | AUC |
|---|---|---|---|---|---|
| Logistic Regression | 0.86 | 0.69 | 0.78 | 0.89 | 0.94 |
| Decision Tree | 0.83 | 0.63 | 0.77 | 0.86 | 0.94 |
| Gradient Boosting | 0.91 | 0.79 | 0.86 | 0.94 | 0.97 |
| Random Forest | 0.92 | 0.79 | 0.87 | 0.94 | 0.98 |

The Receiver Operating Characteristic (ROC) curve analysis provides further insight into the performance of binary classification at various discrimination thresholds. The ROC curve in Figure 16 shows the relation between true positive rate (probability of correctly predicting SRP issues) and false positive rate (probability of falsely predicting issues while the SRP operates normally) cases. The higher area under the precision-recall curve (AP) indicates both high recall and high precision (Pedregosa 2011). The AUC and AP results prove Random Forest to be the best classifier among the four techniques. The classification models serve as a prototype predictive mode and could be improved by simulating more cases in the facility, and more importantly, by using the other lab or field-scale data.

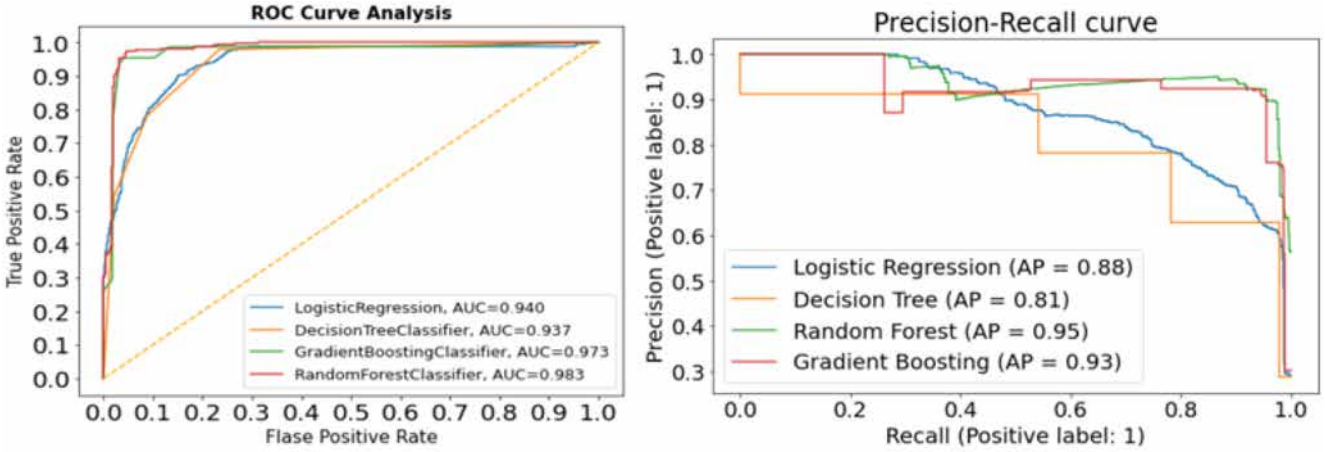


**Figure 16—ROC curve analysis and Precision-Recall (AP) curves for the classification techniques**

## Deployment: Explainable Machine Learning

The final stage of supervised learning is to analyze and quantify the importance of experimental parameters. The feature importance decodes the 'black-box machine learning' and explains how these features generate confidence in the model. The Shapley values, calculated by using Shapley Additive Explanation, indicate the importance of each predictor in predicting a label of 0 or 1. In the statistical context, the Shapley values represent the average of marginal contribution across all combinations of features (Lundberg and Lee 2016, Tran et al. 2020, Lam Tran et al. 2020). This method helps the operators determine key physical parameters for predictive modes in production systems.

The total water column being pumped per minute, intake pressure, and pressure difference between the top and discharge sensors are the top three predictors in determining labels 0 and 1, as shown in Figure 17. This verifies the selection of multiplication of SPM and stroke length and the changing rate of intake pressure with time as determining factors in labeling SRP condition. As the pump operates under the stabilized conditions, the performance is independent of time, making the time feature not as important as the other entities. The rod load ($\Delta F$) indicator is anticipated to be the primary factor in an actual field scenario. However, the dynocard transformation results imply the presence of buckling in the rod string and possibly significant uncertainties in the pump card data. For the case of this study, the rod load factor is not a significant contributor to classify normal and slightly pumped-off classes.

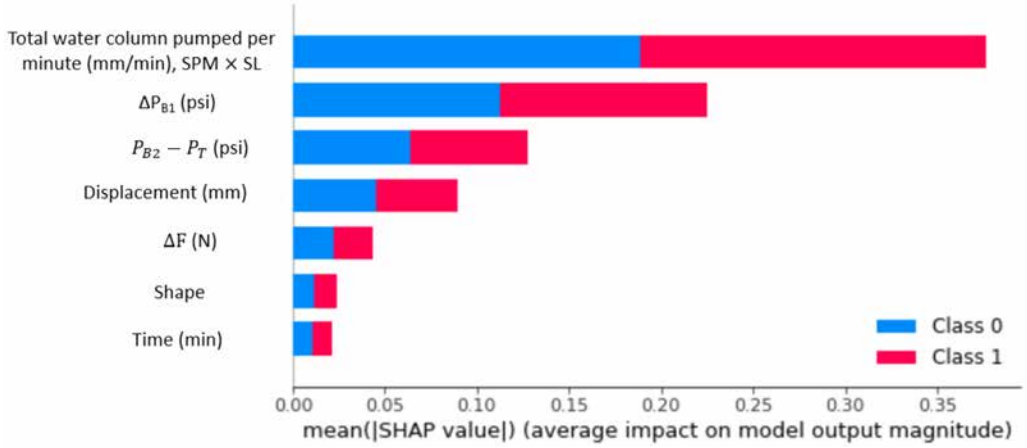


**Figure 17—Variable importance plot based on Shapley values for normal operation (Class 0) and slightly pumped-off anomaly (Class 1)**

Analyzing Shapley values for each label helps in understanding the impacts of operational parameters on SRP conditions. The tornado chart in Figure 18 displays the Shapley values or the significance of all predictors on abnormal card labels in descending order. The colors also represent the intensity of the parametric features. For each predictor, the higher Shapley value means a higher tendency for a pumping-off situation. Therefore, the cases with a higher pumping-off possibility mostly include higher total water column being pumped per minute (SPM × Stroke Length), higher intake pressure changing slope, and higher differential pressure cases. A high total water column being pumped per minute is a key attribute for abnormal cards. The results confirm the underlying physical basis of predictive models in categorizing operational type for IDSRP.

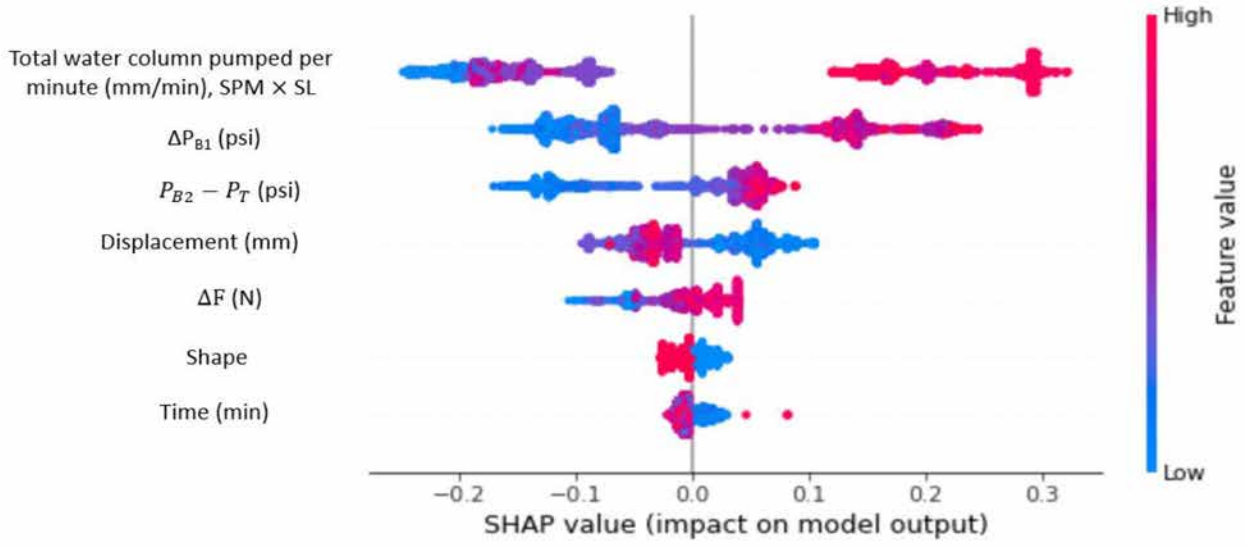


**Figure 18—Shapley values for label 1 or slightly pumped-off data, varying with different predictors**

## Conclusions

This study is an attempt to implement a generic digital design to monitor and diagnose SRP operations. By validating a physical baseline model, the digital laboratory setup has achieved a practical capability to record large datasets of surface dyno cards. Gibbs equation is replicated to transform surface to downhole dynamometer cards. Experimental uncertainties including the rod string buckling during the movement, resulting in card noises during the transition from upstroke to downstroke, are also pointed out.

Machine learning algorithms are used to better predict anomalies in SRP and the impacts of the input parameters. These models achieve evaluation scores from 0.54 to 0.87, with KNN being the best model. The low error between predicted and true outputs demonstrates the strong correlation between the machine learning model and actual operation. The label validation proves the ability of analytical solutions to detect the slightly pumped-off cards. The threshold parameter testing from supervised classification models shows accuracies up to 92% for the dataset, with random forest being the optimal classifier. The results improve the confidence in identifying SRP failures. Experimental inputs can be used as predictors to monitor the SRP performance and detect anomalies by forecasting pressure and load trends with time. Cases with a higher pumping-off possibility mostly include higher water column being pumped per minute, higher intake pressure changing slope with time, and higher tubing pressure gradient cases.

The data sets generated by the setup and the analytical solutions developed in this study show the benefits of combining the physical SRP operation and IoT, cloud data storage, and processing. This study mimics the field operations and produces digital solutions that can be broadly applied without costly software processors.

## Nomenclature

| | |
|---|---|
| $q$ | Liquid flow rate delivered by plunger pump. STB/D |
| $B_o$ | Formation volume factor, rb/STB |
| $E_v$ | Volumetric efficiency of the plunger |
| $S_p$ | Effective plunger stroke length, in |
| $A_p$ | Gross plunder cross-sectional area, in$^2$ |
| $e_r$ | Rod stretch, in |
| $e_t$ | Tubing stretch, in |
| $e_o$ | Plunger over-travel, in |
| $S$ | Stroke length, in |
| $P_{B_1}$ | First bottom gauge (B1) pressure, psig |
| $P_{B_2}$ | Second bottom gauge (B1) pressure, psig |
| $P_T$ | Top gauge (T) pressure, psig |
| $\Delta P_{B1}$ | Difference between maximum and minimum intake pressures per cycle, psi |
| $\Delta F$ | Difference between maximum and minimum rod load in each cycle, N |
| $\Delta$P | Differential pressure between bottom and top gauge, psi |
| $\Delta P_{friction}$ | Frictional pressure drop, psi |
| $R^2$ / R-2 | Coefficient of determination |
| LR | Linear Regression |
| KNN | K-nearest neighbor |
| DT | Decision Tree |
| RMSE | Root mean-square error |
| MSE | Mean-square error |
| MAE | Mean absolute error |
| AUC | Area under Receiver Operating Characteristic curve |
| AP | Area under precision-recall curve |

## References


Abdalla, R., El Ela, M.A. and El-Banbi, A., 2020. Identification of downhole conditions in sucker rod pumped wells using deep neural networks and genetic algorithms. *SPE Production & Operations*, **35**(02), pp.435–447.

Bello, O., E. P. Dolberg, C. Teodoriu, H. Karami, and D. Devegowdva. "Transformation of academic teaching and research: Development of a highly automated experimental sucker rod pumping unit." *Journal of Petroleum Science and Engineering* **190** (2020): 107087.

Bezerra, Marco AD, Leizer Schnitman, Manuel de A. Barreto, A. M. Jose Filho, and Felippe de Souza. "Pattern Recognition for Downhole Dynamometer Card in Oil Rod Pump System Using Artificial Neural Networks." In *ICEIS* (2), pp. 351–355. 2009.

Boguslawski, Bartosz, Matthieu Boujonnier, Loryne Bissuel-Beauvais, Fahd Saghir, and Rajesh D. Sharma. "IIoT edge analytics: Deploying machine learning at the wellhead to identify rod pump failure." In SPE Middle East Artificial Lift Conference and Exhibition. OnePetro, 2018.

Chen, Zengshi, Luther W. White, and Huimin Zhang. "Predicting sucker-rod pumping systems with Fourier series." *SPE Production & Operations* **33**, no. 04 (2018): 928–940.

Derek, H. J., J. W. Jennings, and S. M. Morgan. "Sucker rod pumping unit diagnostics using an expert system." In Permian Basin Oil and Gas Recovery Conference. OnePetro, 1988.

Dickinson, Roderick R., and James W. Jennings. "Use of pattern-recognition techniques in analyzing downhole dynamometer cards." *SPE Production Engineering* **5**, no. 02 (1990): 187–192.

Everitt, Thomas Aaron, and J. W. Jennings. "An improved finite-difference calculation of downhole dynamometer cards for sucker-rod pumps." *SPE production engineering* **7**, no. 01 (1992): 121–127.

Ercolino, J (2011) *Calculation of Downhole Dynamometer Cards for Sucker-Rod Pumps Finite Difference Wave Equation Diagnostic Analysis for Sucker-Rod Pumps*. (Version 1.0.0.0) https://www.mathworks.com/matlabcentral/fileexchange/32342-calculation-of-downhole-dynamometer-cards-for-sucker-rod-pumps

Gibbs, S.G. and Neely, A.B.: "Computer Diagnosis of Down-Hole Conditions In Sucker Rod Pumping Wells," *JPT* (Jan. 1966) 91–98; Trans., AIME, 237.

Gibbs, S. G. "Design and diagnosis of deviated rod-pumped wells." In SPE Annual Technical Conference and Exhibition. OnePetro, 1991.

Kendrick, John F., and Paul D. Cornelius. "The Sucker-rod Pump as a Problem in Elasticity." *Transactions of the AIME* **123**, no. 01 (1937): 15–31.

Lam Tran, Ngoc, Ishank Gupta, Deepak Devegowda, Hamidreza Karami, Chandra Rai, Vikram Jayaram, and Carl Sondergeld. "Machine Learning Workflow to Identify Brittle, Fracable and Producible Rock in Horizontal Wells Using Surface Drilling Data." In SPE Annual Technical Conference and Exhibition. OnePetro, 2020.

Lima, F. S., L. A. Guedes, and D. Silva. "Comparison of Border Descriptors and Pattern Recognition Techniques Applied to Detection and Diagnosis of Faults on Sucker-Rod Pumping System." *Digital Image Processing*. Rijeka, Croatia: InTechOpen (2012).

Liu, Feilong, and Anilkumar Patel. "Well failure detection for rod pump artificial lift system through pattern recognition." In International Petroleum Technology Conference. OnePetro, 2013.

Liu, Shuping, Cauligi S. Raghavendra, Yintao Liu, K. Yao, Oluwafemi Balogun, Lanre Olabinjo, Ram Soma et al. "Automatic early fault detection for rod pump systems." In SPE annual technical conference and exhibition. OnePetro, 2011.

Liu, Yintao, K. Yao, Shuping Liu, Cauligi Srinivasa Raghavendra, Tracy Lynn Lenz, Lanre Olabinjo, B. Seren, Sanaz Seddighrad, and C. G. Dinesh Babu. "Failure prediction for rod pump artificial lift systems." In SPE Western Regional Meeting. OnePetro, 2010.

Lukasiewicz, S. A., and C. Knight. "On lateral and helical buckling of a rod in a tubing." *Journal of Canadian Petroleum Technology* **45**, no. 03 (2006).

Lundberg, Scott M., and Su-In Lee. "A unified approach to interpreting model predictions." *Advances in neural information processing systems* **30** (2017).

Martinez, E. R., W. J. Moreno, V. J. Castillo, and J. A. Moreno. "Rod pumping expert system." In Petroleum Computer Conference. OnePetro, 1993.

Mohammadpoor, Mehdi, Kh Shahbazi, Farshid Torabi, and A. Qazvini. "A new methodology for prediction of bottomhole flowing pressure in vertical multiphase flow in Iranian oil fields using artificial neural networks (ANNs)." In SPE Latin American and caribbean petroleum engineering conference. OnePetro, 2010.

Nazi, G. M., Kaveh Ashenayi, J. F. Lea, and Frank Kemp. "Application of artificial neural network to pump card diagnosis." *SPE Computer Applications* **6**, no. 06 (1994): 9–14.

Osman, El-Sayed A., Mohammed Abdalla Ayoub, and Mohamed Ahmed Aggour. "An artificial neural network model for predicting bottomhole flowing pressure in vertical multiphase flow." In SPE middle east oil and gas show and conference. OnePetro, 2005.

Palmer, Tyler, and Mark Turland. "Proactive rod pump optimization: Leveraging big data to accelerate and improve operations." In SPE North America Artificial Lift Conference and Exhibition. OnePetro, 2016.

Pedregosa, Fabian, Gaël Varoquaux, Alexandre Gramfort, Vincent Michel, Bertrand Thirion, Olivier Grisel, Mathieu Blondel et al. "Scikit-learn: Machine learning in Python." *The Journal of machine Learning research* **12** (2011): 2825–2830.

Pennel, Mike, Jeffrey Hsiung, and V. B. Putcha. "Detecting failures and optimizing performance in artificial lift using machine learning models." In SPE Western Regional Meeting. OnePetro, 2018.

Pienknagura Dolberg, Erik. "Implementation of a Digital Sucker Rod Pumping Unit for Research and Educational Purposes." (2019).

Pons, Victoria. "Optimal stress calculations for sucker rod pumping systems." In SPE Artificial Lift Conference & Exhibition-North America. OnePetro, 2014.

Rashidi, Fariborz, Ehsan Khamehchi, and Hanieh Rasouli. "Oil field optimization based on gas lift optimization." *ESCAPE20* **6** (2010).

Rogers, J. D., C. G. Guffey, and W. J. B. Oldham. "Artificial neural networks for identification of beam pump dynamometer load cards." In SPE Annual Technical Conference and Exhibition. OnePetro, 1990.

Rowlan, O. L., and J. N. McCoy. "Pump Card Reference Load Lines Used for Analysis and Troubleshooting." In SPE Production and Operations Symposium. OnePetro, 2015.

Sharma, Aditya, Opeyemi Bello, Catalin Teodoriu, and Hamidreza Karami. "Design and Implementation of a Laboratory Sucker Rod Pumping Unit Using Industry 4.0 Concepts." *Journal of Energy and Power Technology* **3**, no. 2 (2021): 1–1.

Teodoriu, C., Bello, O., Karami, H. and Devegowda, D. *Automated Data-driven Systems for Predictive Diagnostic in Sucker Rod Pumps*. University of Oklahoma, 2020.

Teodoriu, Catalin, and Erik Pienknagura. "Bringing the sucker rod pumping unit into the classroom with the use of the internet of things." In SPE Annual Technical Conference and Exhibition. OnePetro, 2018.

Tran, Ngoc Lam, Ishank Gupta, Deepak Devegowda, Vikram Jayaram, Hamidreza Karami, Chandra Rai, and Carl H. Sondergeld. "Application of Interpretable Machine-Learning Workflows To Identify Brittle, Fracturable, and Producible Rock in Horizontal Wells Using Surface Drilling Data." *SPE Reservoir Evaluation & Engineering* **23**, no. 04 (2020): 1328–1342.

Tran, Ngoc Lam. "A Data-Driven Approach For Monitoring And Predictive Diagnosis Of Sucker-rod pump System." (2022).

Tripp, H. A. "A review: analyzing beam-pumped wells." *Journal of petroleum technology* **41**, no. 05 (1989): 457–458.

Yu, Yunhua, Haitao Shi, and Lifei Mi. "Research on feature extraction of indicator card data for sucker rod pump working condition diagnosis." *Journal of Control Science and Engineering* **2013** (2013).

Xu, Peng, Shijin Xu, and Hongwei Yin. "Application of self-organizing competitive neural network in fault diagnosis of suck rod pumping system." *Journal of Petroleum Science and Engineering* **58**, no. 1-2 (2007): 43–48.